Scientific Research Journal,
Vol 21 No 1 (2024) 67-82
https://doi.org/10.24191/srj.v21i1.25160

Effect of Pr^{3+} Substitution at the A-Site on the Structural and Electrical Properties of Hole-Doped La-Based Manganites

Rozilah Rajmi[1,*], Norazila Ibrahim[2], Suhadir Shamsuddin[3], Shahrulnizam Md Salleh[4], Muhamad Hazri Othman[4]

[1]Faculty of Applied Sciences, Universiti Teknologi MARA (UiTM) Cawangan Perlis,Kampus Arau, 02600 Arau, Perlis, Malaysia
[2]Faculty of Applied Sciences, Universiti Teknologi MARA (UiTM), 40450 Shah Alam, Selangor, Malaysia.
[3]Faculty of Applied Sciences and Technology,Universiti Tun Hussein Onn Malaysia (UTHM), Pagoh Campus, 84600 Pagoh, Muar, Johor Darul Ta'zim, Malaysia
[4]Industrial Centre of Innovation in Advance Materials, SIRIM Industrial Research, Lot 34 Jalan Hi-Tech 2/3, Kulim Hi-Tech Park, 09000 Kulim Kedah, Malaysia

**Corresponding author's E-mail: rozilahrajmi@uitm.edu.my*

Received: 22 December 2023
Accepted: 10 January 2024
Onlin First: 01 March 2024

ABSTRACT

In this study, the effect of praseodymium substitution at La-site on structural and electrical transport properties of $La_{0.5}Ba_{0.5}MnO_3$ was investigated. Polycrystalline $La_{0.5-x}Pr_{0.5x}Ba_{0.5}MnO_3$ (x = 0, 0.50, 1.00) were synthesized using a conventional solid-state method. The powder X-ray diffraction patterns show a single-phase orthorhombic distorted perovskite structure with space group Pnma. The Rietveld refinement analysis showed that the unit cell volume decreased as Pr^{3+} substitution increased which may be attributed to the different ionic radii of ions. Electrical resistivity measurements by using standard four-point probe resistivity measurement in a temperature range of 30 K to 300 K. As the Pr^{3+} concentration increases, metal-insulator transition, T_{MI} decreases from 264K (x=0) to 157K (x=1.00) while resistivity increases from 1.16 Ω.cm (x = 0) to 20.3 Ω.cm (x =1.00). The decreased T_{MI} are attributed to the decrease in tolerance factor which indicates enhancement in MnO_6 octahedral distortion consequently reduce double exchange interaction. The electrical resistivity in the metallic region for all samples was fitted with the combination of domain/

grain boundary, electron-electron, electron-magnon and electron-phonon scattering processes. The resistivity behaviour in the insulating region for all samples was attributed to small polaron hopping model which revealed that the activation energies increased as Pr^{3+} content increased due to the enhancement in the distortion of MnO_6 octahedral.

Keywords: Manganese Perovskites; Scattering Model; Hoping Model; Lattice Distortion; Electrical Properties.

INTRODUCTION

Extensive research has been undertaken on manganites with the perovskite ABO_3-type structure, specifically those doped with holes, and characterized by the general formula $R_{1-x}A_xMnO_3$ (where R denotes rare earth elements and A represents alkali or alkaline elements). These materials showcase notable characteristics, including colossal magnetoresistance (CMR), a transition from ferromagnetic to paramagnetic states (FM-PM), and a shift from a metallic to an insulator state (MI)[1-5]. These distinctive properties emerge from the double-exchange (DE) interaction, which favors a ferromagnetic-metallic (FMM) state [5-6]. Conversely, the Jahn-Teller (JT) interaction, attributted to Mn^{3+} ions, encourages a paramagnetic insulating (PMI) behaviour [6]. To grasp the physical behaviour of doped manganites comprehensively, it is essential to take into account various additional factors, such as phase separation (PS) [7-8], superexchange (SE) interaction [9], Griffith phase (GP) [10-12], and charge ordering (CO) [8,13].

Correlation between electrical conduction and ferromagnetism in manganites arises from DE interaction where the oxygen mediate coupling of two Mn ions of different valence states between Mn spins [4, 5-7]. The magnetic behaviour in the case of doped manganites is due to two simultaneous transfer of two electrons; one from the Mn^{3+} (d^4,$t_{2g}^{\ 3}$ $e_g^{\ 1}$, S=2) to 2p orbital of O^{2-} while the other is from O^{2-} to an empty eg orbital of Mn^{4+} (d^3,$t_{2g}^{\ 3}$ $e_g^{\ 0}$, S=3/2). Consequently, it enables the eg electrons to move throughout the lattice. The DE interaction depends on the angle between Mn spins where it is strongly affected by structural parameters such as Mn-O-Mn bond angle. The transfer probability of the eg electron, to move from Mn^{3+} to neighbouring Mn^{4+} is, t= to cos (θ/2), θ being the angle between the Mn

spins. The transfer probability varies from 1 for $\theta = 0^o$ to zero for $\theta = 180^o$. If the manganese spins are not parallel, the electron transfer will become more difficult and the mobility decrease [14-16]. In contrast, if manganese spins are parallel, the electrons transfers will be easier. Thus, the mechanism which leads to enhanced electrical conductivity requires a ferromagnetic coupling. This leads to simultaneous occurrence of ferromagnetism and metallicity in the material [17].

Recent studies suggest that the observed behavior in these systems cannot be solely explained by double exchange. Factors such as the average size of A and B site cations, the mismatch effect, and the presence of vacancies in A and B sites play critical roles [18-26]. In doped rare earth manganites, the Mn^{3+}/Mn^{4+} ratio significantly influences the compounds' physical properties, especially their transport properties. However, the precise nature of the DE mechanism, particularly in A-site substitution, remains unclear. It is proposed that substitution with different ionic radii of Pr^{3+} at the La-site may induce lattice distortion and impact the DE interaction. Although this substitution's effect has been reported in manganites, there are fewer reports on the formation of lattice distortion in La-based manganites.

This study investigates the impact of substituting Pr^{3+} at the La-site on the structural and electrical transport characteristics of $La_{0.5-x}Pr_{0.5x}Ba_{0.5}MnO_3$ (x = 0, 0.50, 1.00) manganite. The decrease in τ resulting from the substitution with the larger ionic radius of Pr^{3+} is examined to understand the mechanism behind the double exchange (DE) process. The alterations in resistivity behavior in both metallic and insulating regions due to Pr^{3+} doping are analyzed using scattering and polaron hopping models, respectively.

METHODOLOGY

Polycrystalline samples of $La_{0.5-x}Pr_{0.5x}Ba_{0.5}MnO_3$ (x = 0, 0.50, 1.00) were synthesized through the conventional solid-state method. High-purity (>99.99%) Pr_6O_{11}, La_2O_3, $BaCO_3$, and MnO_2 powders were precisely weighed in a stoichiometric ratio using an electronic balance for this study. After thorough mixing and grinding for 2 h, the powders were calcined in air at 950 °C for 24 h. Subsequently, the resulting powder was pressed into

pellets (diameter: 13 mm; thickness: approximately 3 mm) under a pressure of about 5 tonnes and sintered in air at 1200 °C for 36 h, followed by slow cooling at a rate of 1 °C/min to attain the desired oxygen stoichiometry.

The structural analysis of the samples was conducted using a PANanalytical model Xpert PRO MPD X-ray diffractometer with Cu-Kα ($\lambda = 0.154$ nm) radiation at room temperature. Data collection was performed in the 2θ range of 20 °- 90 °.

The electrical resistivity properties were examined utilizing the standard four-point probe technique over a temperature range of 30–300 K in a Janis model CCS 350ST cryostat under zero external magnetic fields. The resistivity behavior was scrutinized through theoretical scattering and hopping models.

RESULTS AND DISCUSSION

Figure 1 depicts (a) X-ray diffraction (XRD) spectra and (b) final refinement results for $La_{0.5-x}Pr_{0.5x}Ba_{0.5}MnO_3$ (x = 0, 0.50, 1.00) samples at room temperature. The patterns reveal that the peaks of all samples appear at comparable angles and positions, consistent with those previously reported for the parent compound, $La_{0.5}Ba_{0.5}MnO_3$ manganite [16]. In Figure 1(a), the inset spectrum indicates a slight rightward shift in XRD peak intensity towards higher diffraction angles when Pr^{3+} is substituted. This shift is ascribed to the disparity in ionic radius between La^{3+} and Pr^{3+}, causing distortion in the crystalline lattice, a phenomenon consistent with Bragg's equation [17]. This observation aligns with previous findings [17], indicating that a smaller ionic radius of the dopant compared to the host induces peak shifts towards higher diffraction positions due to lattice distortions.

The XRD data underwent refinement using the Rietveld method [27-28], utilizing the General Structure Analysis System (GSAS) program [29], the EXPGUI package, and VESTA [30]. Peak modelling involved a pseudo-Voigt function, and the refinement considered the cell parameter and background function. In Figure 1(b), the XRD patterns of the samples were refined again at room temperature, confirming that all synthesized samples were single-phased and exhibited orthorhombic symmetry with the Pnma

space group. This orthorhombic structure corresponds with prior studies on $La_{0.5}Ba_{0.5}MnO_3$ manganites using the same refinement technique [15].

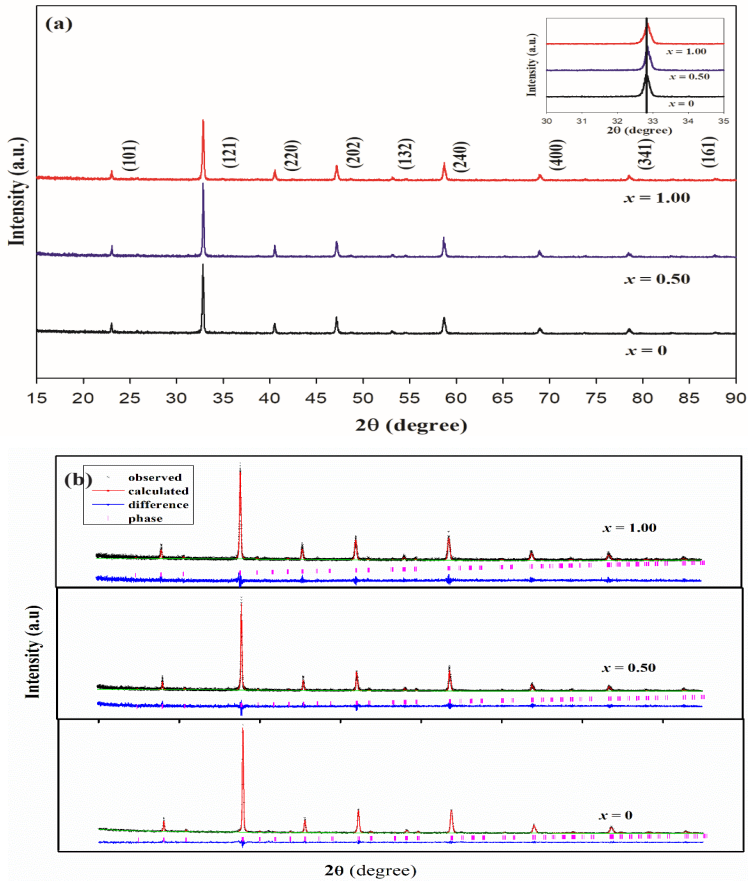

Figure 1(a) presents X-ray diffraction (XRD) spectra at room temperature for $La_{0.5-x}Pr_{0.5x}Ba_{0.5}MnO_3$ (x= 0, 0.50, 1.00) samples. The inset highlights a slightly rightward shift in the XRD spectra due to substitution, particularly noticeable in the position of the prominent peak. For Figure 1(b) displays the final refinement at room temperature for $La_{0.5-x}Pr_{0.5x}Ba_{0.5}MnO_3$ (x= 0, 0.50, 1.00) samples, which is the observed data (cross black), calculated data (continuous red line), the difference between observed and calculated data (blue line), and the positions of Bragg peaks (vertical pink tick marks).

Table 1 presents the lattice parameters, calculated unit cell volume (V), and chi-squared (χ^2) values resulting from the final refinement of $La_{0.5-x}Pr_{0.5x}Ba_{0.5}MnO_3$ (x = 0, 0.50, 1.00) samples. The structural parameter values for the x = 0 sample align with those previously reported [15] for the compound. The χ^2 goodness-of-fit (GOF) indicator indicates a robust agreement between observed and calculated profiles, exemplified by the refinement quality shown in Figure 1(b). The calculated unit cell volume decreases for samples with Pr^{3+} substitution, ranging from 240.40 $Å^3$ (x = 0) to 227.54 $Å^3$ (x = 1.00). This slight reduction in unit cell volume implies the potential replacement of La^{3+} by Pr^{3+} in the crystal structure, attributable to the smaller ionic radius of Pr^{3+} (1.18 Å) [32] compared to that of La^{3+} (1.22 Å) [32].

Table 1: Structure parameters, unit cell volume, goodness of fit value for refinement and Jahn-Teller Variance of $La_{0.5-x}Pr_{0.5x}Ba_{0.5}MnO_3$ (x= 0, 0.50, 1.00) samples. The number in the brackets represents uncertainty of the last digit.

Sample	x =0	x = 0.50	x = 1.00
Lattice parameter			
a (Å)	5.5370(4)	5.5310(2)	5.5180(2)
b (Å)	7.8320(5)	7.8200(3)	7.8000(5)
c (Å)	5.5390(2)	5.5320(6)	5.5190(6)
Volume, V ($Å^3$)	240.20(2)	239.23(5)	227.54(3)
Goodness of fit, χ^2	1.0430	1.5500	1.5410
Jahn-Teller Variance, $\sigma_{JT}{}^2$($x10^{-5}$ $Å^2$)	0.6130	0.6254	0.6305
Tolerance factor, τ (nm)	0.9341	0.9216	0.9195

The magnitude of MnO_6 octahedral distortion was determined by calculating the variance in JT denoted by σ^2_{JT}. This was achieved using Eq. (1) [33-34]:

$$\sigma_{JT}^2 = 1/6 \sum[d_{(Mn-O)i} - d_{<Mn-O>} / d_{<Mn-O>}]^2 \quad (1)$$

Here, $d_{(Mn-O)}$ represents the individual M-O bond distance, and $d_{<Mn-O>}$ represents the average Mn-O bond distance. The calculated values of σ^2_{JT} showed a increase for substituted sample.

Further, to verify the structural stability of the samples, tolerance factor (τ) is calculated using Eq. (2) [33-34] which is given by:

$$\tau = (r_A + r_o)/\sqrt{2}(r_B + r_o) \quad (2)$$

where (r_A) is average ionic radii of A site, (r_B) is average ionic radii of B site and r_O is average ionic radii of O site. The τ values were calculated according to Shannon values [32] with coordination 9 which varies from 0.9341 (x = 0) to 0.9195 (x = 1.00), as tabulated in Table 1.The decreased value of the tolerance factor, τ, with Pr^{3+} content (Table 1) indicates an increase in lattice mismatch between the A-O and its neighboring B-O layers. This increase is caused by the distortion of the MnO_6 octahedral, resulting in decreased Mn^{3+}-O-Mn^{4+} bond angles. Consequently, electron hopping is reduced and charge localization is enhanced. The Mn-O and Mn^{3+}-O-Mn^{4+} bond angles are particularly interesting because they play a crucial role in the magnetic and transport properties of manganites.

Resistivity against temperature, ρ(T) curves under zero external magnetic fields over a temperature range of 20 K–300 K for $La_{0.5-x}Pr_{0.5x}Ba_{0.5}MnO_3$ (x= 0, 0.50, 1.00) samples are displayed in Figure 2 All the sample showed MI behaviour with T_{MI} decreased from 264 K (x = 0) to 157 K (x = 1.00) for further Pr^{3+} substitution, as presented in Table 2. The resistivity increased with the increased Pr^{3+} concentration from 1.16 Ω.cm (x = 0) to 20.3 Ω.cm (x =1.00).

The increased resistivity and decreased TMI value as Pr^{3+} substitution (Figure 2 and Table 2) is exhibited the degree of MnO_6 octahedral distortion of the samples increased, as indicated by the increase in σ_{JT}^2 value with Pr^{3+} substitution (Table 2). This behaviour may be attributed to the weakening of DE Mn^{3+}–O–Mn^{4+} interactions due to the increase distortion. Thus, the reduced DE interaction result in increased localization of the charge carriers, as suggested by the resistivity behaviour.

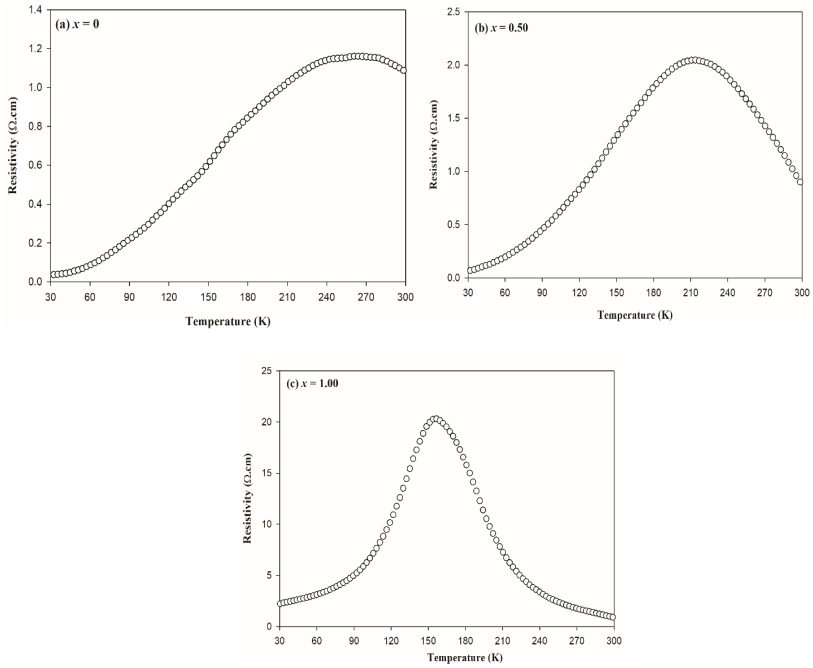

Figure 2: Resistivity versus Temperature Curves for $L_{a0.5-x}Pr_{0.5x}Ba_{0.5}MnO_3$ (x = 0, 0.50, 1.00) under zero Magnetic Field.

Table 2: Metal-Insulator Transition Temperatures (T_{MI}) and Resistivity (ρ) at T_{MI} for $La_{0.5-x}Pr_{0.5x}Ba_{0.5}MnO_3$ (x= 0, 0.50, 1.00) samples under zero Magnetic Field.

Sample	x =0	x= 0.50	x = 1.00
T_{MI} (K)	264	214	157
ρ at T_{MI} (Ω.cm)	1.16	2.04	20.3

In order to understand the conduction mechanism involved in the resistivity behaviour of $La_{0.5-x}Pr_{0.5x}Ba_{0.5}MnO_3$ (x= 0, 0.50, 1.00) manganites in the metallic region ($T<T_{MI}$), the resistivity data in the region under zero magnetic field (Figure 3) were fitted using Eq. (3) [32].

$$\rho = \rho_0 + \rho_{2.5}T^{2.5} \quad (3)$$

where ρ_0 term arises due to the grain/domain boundary and $\rho_{2.5} T^{2.5}$ is combination of electron-electron, electron-magnon and electron-phonon scattering processes [27-28, 31] The squared value of linear coefficient (R^2) value is high at 99.97 % for Eq. (3) which represents the best fitting quality. All the fitted parameter values for all samples are given in Table 3. All the fitting parameters, namely, ρ_0 and $\rho_{2.5}$ increased with Pr^{3+} substitution. Such increase indicates that Pr^{3+} substitution increased the electron–electron interaction, electron-magnon and electron–phonon scatterings.

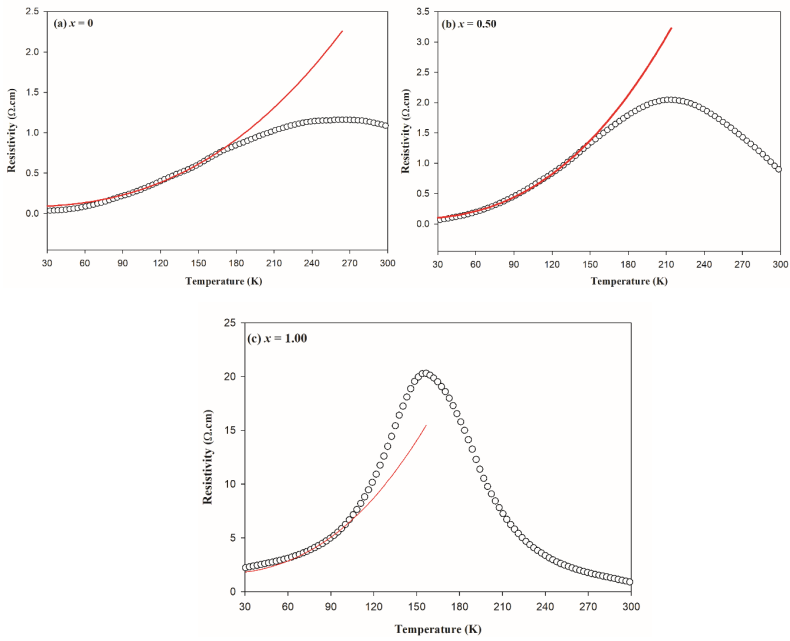

Figure 3: Temperature Dependence of Resistivity under Magnetic Fields 0 T $La_{0.5-x}Pr_{0.5x}Ba_{0.5}MnO_3$ (x= 0, 0.50,1.00). The Solid Lines Show the Fitting Made to $\rho = \rho_0 + \rho_{2.5}T^{2.5}$

Table 3: Fitted parameters obtained from fitting experimental data at low temperature in the metallic region and Activation energy, Ea obtained from SPH model fitting in the insulating region for $La_{0.5-x}Pr_{0.5x}Ba_{0.5}MnO_3$ (x= 0, 0.50,1.00) samples.

Sample	x =0	x = 0.50	x = 1.00
Metallic region ($T < T_{MI}$)			
ρ_0 (Ω.cm)	0.0787	0.0827	1.5923
$\rho_{2.5}$ (Ω.cm)	1.9218×10^{-6}	4.7048×10^{-6}	4.5269×10^{-5}
Insulating region ($T > T_{MI}$)			
Activation Energy, E_a (meV)	60.2	139	198

Moreover, the conduction mechanism in the high-temperature insulating region of manganite can be clarified by examining hopping models. The resistivity data in this region is modelled using the Small Polaron Hopping (SPH) model.

Generally, the SPH model is employed to elucidate electron conduction at elevated temperatures, where the electron conduction is connected to thermal activation. At higher temperatures, the thermal energy is adequate to enable electrons to transition to their nearest neighbouring states. The expression for the SPH model is represented by Eq. (4) as follows [27-28]:

$$\rho = \rho_0 T \, exp \, E_a / K_B \tag{4}$$

The activation energy, Ea values for SPH increased with increasing Pr^{3+} substitution (Table 3), which may be related to the reduction of electron delocalization. The decreased delocalization is caused by enhancement of distortion in MnO_6 octahedral, as indicated by the decrease in τ (Table 1), which thereby decreased carrier hopping [27-28].

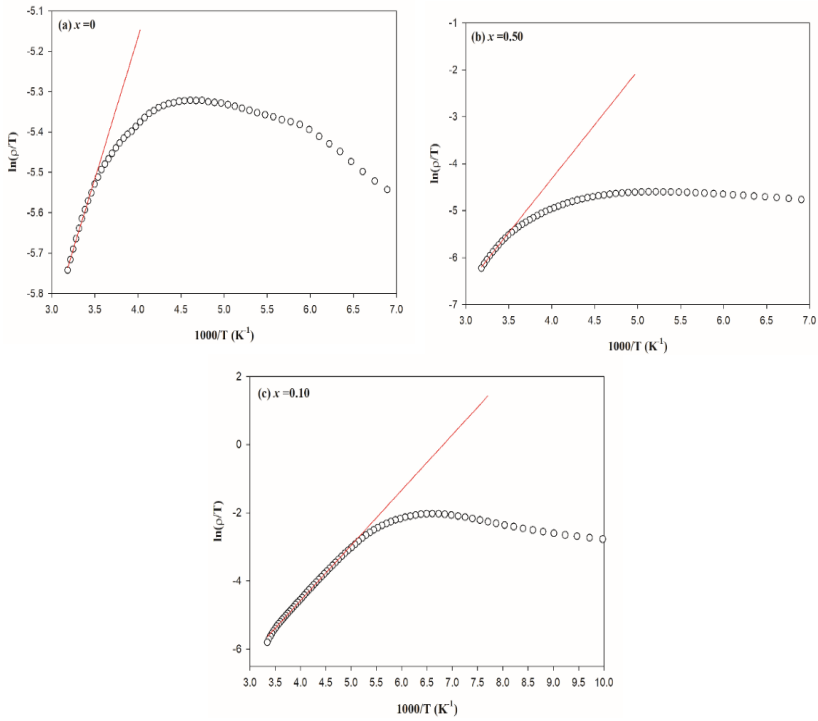

Figure 4: Plot of ln (ρ/T) versus1000/T for $La_{0.5-x}Pr_{0.5x}Ba_{0.5}MnO_3$ (x= 0, 0.50, 1.00) Sample. The Solid Line Indicates the Best-Fit to the SPH Model

CONCLUSION

In conclusion, this study investigated the impact of substituting Pr^{3+} at the La-site in $La_{0.5-x}Pr_{0.5x}Ba_{0.5}MnO_3$ (x = 0, 0.50, 1.00) samples on their structural and electrical transport properties, with a focus on understanding the influence of lattice distortion. The results indicated that the metal-insulator transition (T_{MI}) decreases as the concentration of Pr^{3+} increases. This reduction in T_{MI} is linked to a decrease in the tolerance factor, signifying an enhancement in MnO_6 octahedral distortion, ultimately leading to a decrease in double exchange interaction. The metallic region's electrical resistivity for all samples was analyzed using a combination of domain/grain boundary, electron-electron, electron-magnon, and electron-phonon scattering processes. Additionally, the resistivity behavior in the insulating

region for all samples was attributed to the small polaron hopping model, revealing that activation energies increased with higher Pr^{3+} content due to the intensified distortion of MnO_6 octahedral structures.

ACKNOWLEDGEMENTS

This work was supported by the Malaysian Ministry of Higher Education (MOHE) and Institute of Research Management and Innovation (IRMI), Universiti Teknologi MARA for providing fellowships and facilities to carry out the measurements [Ref: 600-RMC/GPM LPHD 5/3 (070/2021)].

REFERENCES

[1] L.P. Gor'kov & V.Z. Kresin, 2004. Mixed-valence manganites: Fundamentals and main properties. *Physics Reports*, 400, 149-208.

[2] A.Žužić, R. Antonia Ressler & M. Jelena, 2022. Perovskite oxides as active materials in novel alternatives to well-known technologies: A review. *Ceramics International,* 48 (19), 27240-27261.

[3] C. Joël, B. Jean Francois & L. Ulrike, 2005. Development of new materials for spintronics. *Comptes Rendus Physique*. 6, 977-996.

[4] V.E. Salazar-Muñoz, A. Lobo Guerrero, S.A. Palomares-Sánchez, 2022. Review of magnetocaloric properties in lanthanum manganites. *Journal of Magnetism and Magnetic Materials*, 562, 169787.

[5] J.M.D. Coey & M. Viret, 1999. Mixed-valence manganites, *Advances in Physics*, 48, 167-293.

[6] S.Herbert, A. Maignan, C. Martin & B. Raveau, 2001. Important role of impurity eg levels on the ground state of Mn-site doped manganites. *Solid State Communications*, 121, 229-234.

[7] E. Dagotto, T. Hotta & A. Moreo, 2001. Colossal magnetoresistance materials; The key role of phase separation. *Physics Reports*, 344,

1-153.

[8] B. Raveau, M. Herviu, A. Maignan & C. Martin, 2001. The route to CMR manganites: What about charge ordering and phase separation?. *Journal of Materials Chemistry,* 11, 29-36.

[9] C. Zener, 1951. Interaction between the d-Shells in the transition metals. II Ferromagnetic compounds of manganese with perovskite structure. *Journal of Physical Review*, 82, 403-405.

[10] S.O. Manjunatha, A. Rao, P. Poornesh, W.J. Lin & Y.-K. Ku, 2016. Magnetic inhomogeneity and Griffiths phase in Bi substituted $La_{0.65-x}Bi_xCa_{0.35}MnO_3$ manganites. *Physica B,* 498, 82–91.

[11] N. Rama, M. Opel, V. Sankaranarayanan, R. Gross, S.B. Ogale, T. Venkatesan & R. Ramachandra, 2005. A-site dependent percolative thermopower and Griffiths phase in $Pr_{0.7-x}Ho_xSr_{0.3}MnO_3$ (x = 0.0, 0.04, 0.08 and 0.1). J*ournal of Applied Physics*, 97, 13-1–13-3.

[12] H. Yoshizawa , Y. Tomioka & Y. Tokura, 2003. Novel stripe-type charge ordering in the metallic A-type antiferromagnet $Pr_{0.5}Sr_{0.5}MnO_3$. *Physica B*, 329, 79–680.

[13] Y. Tomioka, T. Okuda, Y. Okimoto, A. Asamitsu, H. Kuwahara & Y. Tokura, 2001. Charge/orbital ordering in perovskite manganites. *Journals of Alloys and Compounds*, 326, 27-35.

[14] L.T.T. Ngan, N.T. Dang, N.X. Phuc, L.V. Bau, N.V. Dang, D.H. Manh, P.H. Nam, L.H. Nguyen & P.T. Phong, 2022. Magnetic and transport behaviors of Co substitution in $La_{0.7}Sr_{0.3}MnO_3$ perovskite. *Journal of Alloys and Compounds*, 911,164967.

[15] B. Ravi, S.R. Shinde, K.M. Gapchup, K.P. Adhi, S.I. Patil, 2003. Effect of aluminum doping on the magneto-transport properties of $La_{0.75}Ca_{0.25}MnO_3$. *Journal of Magnetism and Magnetic Material,* 256, 425 – 429.

[16] M. Iqbal, M. Nasir Khan, A. A. Khan, I. Zaka, S. Hussain, M. S. Ch & A. Mehmood, 2017. Structure and charge transport mechanism in hydrothermally synthesized ($La_{0.5}Ba_{0.5}MnO_3$) cubic perovskite manganite, *Journal of Materials Science: Materials in Electronics,* 28:15065–15073.

[17] B. Rajesh Kumar & B. Hymavathi, 2017. X-ray peak profile analysis of solid-state sintered alumina doped zinc oxide ceramics by Williamson–Hall and size-strain plot methods. *Journal of Asian Ceramic Societies,* 5(2), 94-103.

[18] A.Žužić, L.Pavić, A. Bafti, S. Marijan, J. Macan & A. Gajović, 2023. The role of the A-site cation and crystal structure on the electrical conductivity of strontium-doped calcium and barium manganites. *Journal of Alloys and Compounds,* 935, 67949.

[19] B. Sudakshina, M.V Suneesh, B. Arun, D. Chandrasekhar Kakarla & M. Vasundhara, 2022. Effects of Cr,Co,Ni substitution at Mn-site on structural, magnetic properties and critical behaviour in $Nd_{0.67}Ba_{0.33}MnO_3$ mixed-valent manganite. *Journal of Magnetism and Magnetic Materials*, 548, 168980

[20] L.Liu, Z.Zou, B.He, Z.Mao & Z.Xie, 2022. Effect of Bi doping on the crystal structure, magnetic and magnetocaloric properties of $La_{0.7-x}Bi_xSr_{0.15}Ca0_{.15}MnO_3$ (x = 0, 0.05, 0.10, 0.15) manganites. *Journal of Magnetism and Magnetic Materials,* 549,169006.

[21] Z. Jira′ k, F. Damay, M. Hervieu, C. Martin, B. Raveau, G. Andre′ & F. Boure′, 2000. Magnetism and Charge Ordering in $Pr_{0.5}Ca_xSr_{0.5-x}MnO_3$ (x = 0.09 and 0.5). *Physical Review B*, 61, 1181- 1188.

[22] M. Jaime, P. Lin, M. B. Salamon and P. D. Han, 1998. Low-Temperature Electrical Transport and Double Exchange in $La_{0.67}(Pb,Ca)_{0.33}MnO_3$. *Physical Review. B*, 58, 5901-5904.

[23] D.Ping, C. Zhenghao, D. Shouyu & Z. Yueliang, 2004. $La_{0.7}Pr_{0.3}MnO_3$ ceramic: An electron-doped colossal magnetoresistive manganite. *Applied Physics Letters* 84, 4741-4743.

[24] J.Li, H.Wang, Z.Liang, Y.Li, Q.Chen, H.Zhang & Y.Li, 2022. Improvement of electrical and magnetic properties in $La_{0.67}Ca_{0.33}Mn_{0.97}Co_{0.03}O_3$ ceramic by Ag doping. *Ceramics International,* 48(24), 36888-36899

[25] L Pi, S. H´ebert, C. Yaicle, C. Martin, A. Maignan & B. Raveau, 2003. The $Pr_{0.5}Ca_{0.5}Mn_{1-x}Cr_xO_3$ series ($0 \leq x \leq 0.5$): evidence of steps in the magnetic and transport properties for a narrow composition range. *Journal of Physics: Condensed Matter,* 135, 2701–2709.

[26] Y.L. Zhu, 2007. Microstructural and magnetic properties of bulk $La_{1-x}Pr_xMnO_3$(x = 0.2, 0.3, 0.5). *Philosophical Magazine Letters,* 87, 75-83.

[27] M.Arifin, N. Ibrahim, Z. Mohamed, A. K. Yahya, Nawazish A. Khan & M. Nasir Khan, 2018. Revival of Metal-Insulator and Ferromagnetic-Paramagnetic Transitions by Ni Substitution at Mn Site in Charge-Ordered Monovalent Doped $Nd_{0.75}Na_{0.25}MnO_3$ manganite. *Journal of Superconductivity and Novel Magnetism*, 1-18.

[28] R. Rozilah, N. Ibrahim, Z. Mohamed, A.K. Yahya, Nawazish A. Khan & M. Nasir Khan, 2017. Inducement of ferromagnetic-metallic phase in intermediate-doped charge-ordered $Pr_{0.75}Na_{0.25}MnO_3$ manganite by K+ substitution. *Physica B: Condensed Matter,* 521, 281–294.

[29] B.H. Toby, 2001. EXPGUI, a graphical user interface for GSAS. *Journal of Applied Crystallography,* 34, 210-213

[30] K. Momma & F. Izumi, 2008. VESTA: A three-dimensional visualization system for electronic and structural analysis. *Journal of Applied Crystallography*, 14, 653-658.

[31] E. Elyana, Z. Mohamed, S.A. Kamil, S.N. Supardan, S.K. Chen & A.K. Yahya, 2018. Revival of ferromagnetic behavior in charge-ordered $Pr_{0.75}Na_{0.25}MnO_3$ manganite by ruthenium doping at Mn site and its MR effect. *Journal of Solid State Chemistry,* 258, 191–200.

[32] R.D. Shannon, 1976. Revised effective ionic radii and systematic studies of interatomic distances in Halides and Chaleogenides. *Acta Crystallographica*, 32, 751-767.

[33] F.B.Jemaa, S. Mahmood, M. Ellouze, E.K. Hlil, F. Halouani, I. Bsoul, & M. Awawdeh.2014. Structural, magnetic and magnetocaloric properties of $La_{0.67}Ba_{0.22}Sr_{0.11}Mn_{1-x}Fe_xO_3$ nanopowders. *Journal of Solid State Sciences*, 37: 121-130.

[34] R. Rozilah, N. Ibrahim & A.K. Yahya, 2019. Inducement of ferromagnetic–metallic phase and magnetoresistance behavior in charged ordered monovalent-doped $Pr_{0.75}Na_{0.25}MnO_3$ manganite by Ni substitution. *Solid State Sciences,* 87, 64-80.